Molecule-by-Molecule Writing Using a Focused Electron Beam

Willem F. van Dorp,[†,*] Xiaoyan Zhang,[‡] Ben L. Feringa,[‡] Thomas W. Hansen,[§] Jakob B. Wagner,[§] and Jeff Th. M. De Hosson[†]

[†]Applied Physics, Zernike Institute for Advanced Materials, University of Groningen, Nijenborgh 4, 9747 AG Groningen, The Netherlands, [‡]Zernike Institute for Advanced Materials and Stratingh Institute for Chemistry, University of Groningen, Nijenborgh 4, 9747 AG Groningen, The Netherlands, and [§]Center for Electron Nanoscopy, Technical University of Denmark, Fysikvej, DK-2800 Kongens Lyngby, Denmark

ABSTRACT The resolution of lithography techniques needs to be extended beyond their current limits to continue the trend of miniaturization and enable new applications. But what is the ultimate spatial resolution? It is known that single atoms can be imaged with a highly focused electron beam. Can single atoms also be written with an electron beam? We verify this with focused electron-beam-induced deposition (FEBID), a direct-write technique that has the current record for the smallest feature written by (electron) optical lithography. We show that the deposition of an organometallic precursor on graphene can be followed molecule-by-molecule with FEBID. The results show that mechanisms that are inherent to the process inhibit a further increase in control over the process. Hence, our results present the resolution limit of (electron) optical lithography techniques. The writing of isolated, subnanometer features with nanometer precision can be used, for instance, for the local modification of graphene and for catalysis.
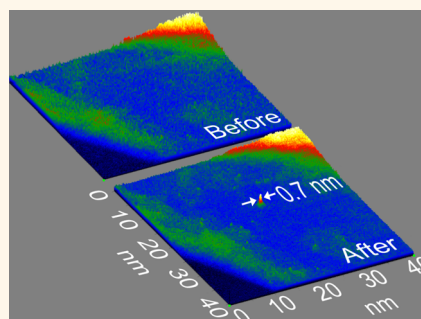
Miniaturization has brought a wealth of applications in the past decades, driven by the developments in the semiconductor industry. Optical lithography with 193 nm wavelength produces circuits with 32 nm features, allowing integrated circuits to contain a million times more transistors than 40 years ago.[1] To continue the trend of miniaturization and enable new applications, the resolution of lithography techniques needs to be stretched beyond their current limits. The ultimate limit in lithography, the manipulation of single atoms, has been demonstrated with the scanning tunneling microscope (STM),[2] which has led to the single atom transistor.[3] However, it remains challenging to apply the deterministic method of picking up and placing atoms on an industrial scale. In comparison, lithography techniques based on (electron) optics are easier to scale. Can the ultimate resolution limit compete with STM writing? The best resolutions of these (electron) optical lithography techniques are compared in Figure 1a. State-of-the-art electron beam lithography (EBL) reaches a resolution of 5 nm by using ultrathin resists.[4] A higher resolution is obtained

with focused electron-beam-induced deposition (FEBID), where a layer of adsorbed precursor molecules is used instead of a resist layer. The deposition of dots with a full width at half-maximum smaller than 1 nm using FEBID has been reported.[5]

Here we present the molecule-by-molecule deposition on few-layer graphene of an organometallic precursor with FEBID. FEBID relies on the dissociation of adsorbed precursor molecules by a focused beam of electrons, working as locally activated chemical vapor deposition. Transiently adsorbed precursor molecules are fragmented in the bombardment with the electrons, and the nonvolatile fragments form the desired deposit (see Figure 1b for a schematic drawing). Generally, the width of a deposit (when created with a stationary electron beam) increases with the exposure time, with wider deposits being created with larger electron doses.[6−8] Therefore, smaller deposits can be obtained simply by decreasing the electron exposure. However, when nanometer-scale deposits are written with FEBID, the process is dominated by Poisson statistics. Provided the size of the deposit is small enough, the
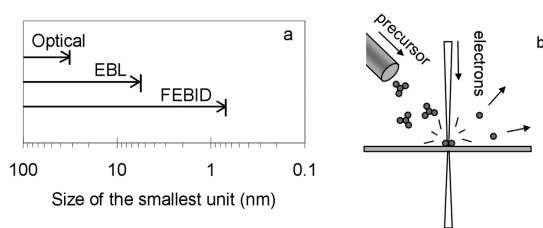
Figure 1. (a) Size of features produced with industrial 193 nm wavelength optical lithography technique, state-of-the-art electron beam lithography (EBL), and focused electron-beam-induced deposition (FEBID). (b) Schematic drawing of FEBID. Precursor molecules, introduced through the nozzle, are dissociated on the substrate surface by electrons. The residue that remains on the surface forms the desired deposit.
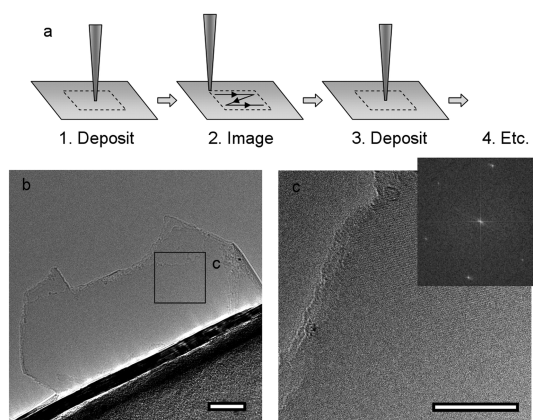

Figure 2. (a) Dedicated scan routine alternates between deposition (stationary positioning of the e-beam on one location) and imaging (rastering over the exposed region). (b) Graphene flake consisting of 4−5 layers. The scale bar indicates 20 nm. (c) Image of the area indicated in (b). The scale bar indicates 10 nm. In the Fourier transform in the inset, the hexagonal diffraction pattern of (few-layer) graphene is visible.

amount of deposited material is not linearly proportional to the electron exposure time but is instead determined by the statistics on the number of dissociated molecules.[9] This makes it impossible to extend the existing strategy of merely decreasing the electron exposure time to reduce the deposit size. If we want to go beyond the current resolution limit, it is necessary to use a technique that compensates for the randomness of the process.

RESULTS AND DISCUSSION

We use a dedicated scan routine for the molecule-by-molecule deposition in a scanning transmission electron microscope (STEM). With a focused electron beam of about 0.3 nm in diameter, we alternate deposition (exposure of the sample by the stationary electron beam) and imaging (rastering over an area of 1.8 by 1.8 nm, centered around the exposed region, pixel size 0.12 nm). During rastering, we collect the transmitted annular dark-field (ADF) signal for Z-contrast imaging, which is registered in V. The intensity of the ADF signal is proportional to the thickness of the sample and the atomic number Z, provided that the (electron-transparent) sample is thin.[10] This enables us to record a movie of the growing deposit and quantify the amount of deposited material in situ.[5] Figure 2a shows a schematic drawing of the iteration procedure. Both the deposition and the imaging are done in the presence of the precursor gas $W(CO)_6$, which is introduced into the microscope at a pressure of 2×10^{-5} mbar.

We use few-layer graphene as the support to avoid undesired broadening of the deposits due to secondary electron emission. Secondary electrons are generated by the incident (primary) electrons in the support and play a dominant role in the dissociation process. We observe that on amorphous carbon membranes, which are typically between 5 and 30 nm thick, the first nuclei that form the base of the deposits are distributed over an area that is larger than the frames of the growth movies. This is the case even for amorphous carbon membranes as thin as 1 nm and for graphene oxide. This behavior is consistent with the emission of

secondary electrons from the support, which have attenuation lengths of 1 nm or more at an energy below 7 eV.[11] This inherent limitation of the amorphous membranes is avoided by using graphene as support. Graphene is the thinnest support material available for TEM experiments, so that broadening of the deposit due to secondary electron emission is negligible. It has the additional benefit of offering excellent contrast for the imaging of nanodeposits created from $W(CO)_6$.[12]

Prior to the deposition, the microscope and sample holder are plasma cleaned. After loading the sample, it is annealed in situ at 500 °C for 10 min. During deposition, a liquid-nitrogen-cooled anticontamination device is used to minimize contamination. We have found that this cleaning procedure generally gives optimal deposition conditions, and it enables hours of contamination-free imaging of samples at room temperature. An exception to this is large-area single-layer graphene, which we are not able to image contamination-free. Exhaustive additional cleaning does not reduce the contamination level (see Supporting Information for more details). Therefore, we use few-layer graphene prepared by chemical exfoliation[13−15] as a support for our experiments. Bright-field TEM images of few-layer graphene flakes are shown in Figure 2b,c.

The ADF image in Figure 3a shows the few-layer graphene after the deposition of a nanodot. All ADF images that are shown in this paper are raw data as recorded without image processing being applied. Figure 3b shows the ADF signal as a function of time; each data point represents the integrated intensity of a single frame. The ADF signal decreases slightly for the first 3.5 s, before it starts to increase. We attribute this initial decrease to the sputtering of the carbon atoms from the few-layer graphene by the 300 keV incident
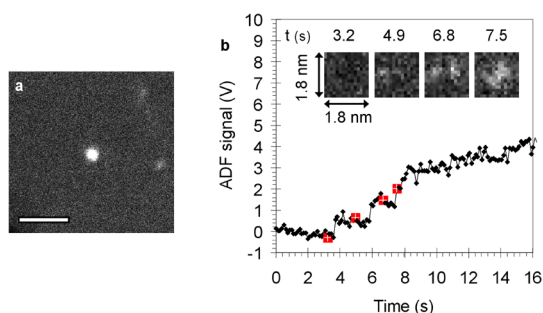
Figure 3. (a) ADF image of the few-layer graphene after the deposition of a nanodeposit. The scale bar indicates 5 nm. (b) Integrated ADF intensities of the images recorded during the growth of the deposit plotted as a function of time. The insets are individual frames from the growth movie.

Figure 4. (a) Histogram of the integrated ADF intensities from the growth movies. The most intense peak, around 0 V, originates from the few-layer graphene. Three peaks, between 0.5 and 3.0 V, are equally spaced at 0.6 V. (b) Histogram of the distribution of the first three step durations. It takes considerably longer to reach the first step than to reach the second or third step.

electrons.[16] Additional examples of the growth curves are shown in the Supporting Information.

The ADF signal in Figure 3b increases in steps. After prolonged exposure, the increase becomes more gradual and steps can no longer be identified. We have collected data from a total of 13 growth experiments in a histogram depicted in Figure 4a. The only form of data treatment we have applied is the removal of the negative slope that is observed at the start of the experiment at times. The data cluster in distinguishable peaks. The first and most intense peak, around 0 V, originates from the few-layer graphene that is imaged and can be considered as the background level. Between 0.5 and 3.0 V, three peaks are observed equally spaced at 0.6 V. These peaks are related to the visible steps in the growth curves.

In the histogram in Figure 4b, the distribution of the step durations is plotted. It is observed that it takes considerably longer to reach the first step (on average 5.6 s) than to reach the second or third step (0.9 and 2.1 s, respectively). This is consistent with the residence time of the precursor molecules, which is longer on the deposit itself than on the virgin graphene. This leads to a higher probability of dissociation and a higher growth rate once the initial deposit has formed.[12]

The step value of 0.6 V is consistent with the expected ADF voltage of a dissociated $W(CO)_6$ molecule. In the experiment, the transmitted electrons are recorded with an annular detector, recording the annular dark-field signal. In the few-layer graphene, the incident electrons undergo single scattering. Therefore, the ADF signal is element-dependent:

$$I_W = I_C(Z_W^{\alpha}/Z_C^{\alpha}) \qquad (1)$$

where I_W and I_C are the signal generated by a tungsten and a carbon atom, respectively, Z is the atomic number, and α is the scattering factor. Values for α, measured and calculated at the collecting angle used in our experiment (68 mrad), are 1.64[17] and 1.74,[10] respectively. Therefore, we conclude that α = 1.69 in our experiment. We calibrate the ADF signal with the lacey carbon membrane from the sample. From earlier
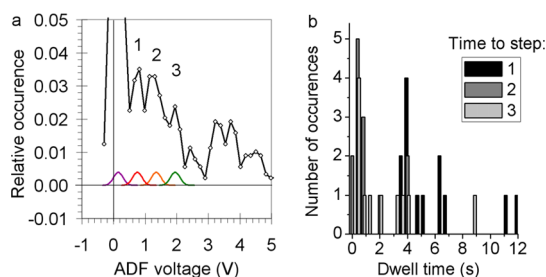
experiments with 1 nm thick membranes,[18] we have determined that the lacey carbon membrane used in the currently described experiments is 31.0 nm thick. In these conditions, the ADF signal is proportional to the membrane thickness, so that it is valid to use the ADF signal for quantification.[17] When imaging this membrane with the standard FEI imaging software, this generates 5.5×10^3 counts, or I_{1nmC} = 176 counts/nm. On the National Instruments card, this is $I_{1nmC} = 8.2 \times 10^{-3}$ V/nm. The number of carbon atoms N exposed to the electron beam in a slice of 1 nm thickness is

$$N = (N_A V_{carbon}\rho \times 10^{-21})/M \qquad (2)$$

where N_A is Avogadro's constant, ρ = 1.7 g/cm^3,[27] and M = 12.01. V_{carbon} is

$$V_{carbon} = \frac{1}{4}\pi d_{beam}^2 \qquad (3)$$

where d_{beam} is 0.3 nm, the diameter of the electron beam. From the calculation, it follows that N = 6. Four carbon atoms/nm contributes to the ADF signal. Combined with the value for I_{1nmC}, this leads to an intensity per C atom of $I_C = 1.3 \times 10^{-3}$ V/atom.

To correlate I_W to the values found in the histogram in Figure 4, we have to take into account that a single W atom sitting on the few-layer graphene is sampled several times by the electron beam. In the experiment, the pixel size is 0.12 nm. The point spread function of the microscope determines the observed diameter of isolated heavy atoms when they are imaged in the STEM.[19] Therefore, the accumulated intensity that represents a single W atom in the growth curves and in the histogram is

$$\Sigma I_W = I_W \frac{1}{4}\pi(0.3/0.12)^2 \qquad (4)$$

This leads to an accumulated intensity ΣI_W = 0.44 V.

However, it is anticipated that $W(CO)_6$ does not decompose to W. Organometallic precursors rarely decompose to pure metal deposits under electron irradiation, and methods to improve the purity after deposition are being studied.[7] Generally, deposits from
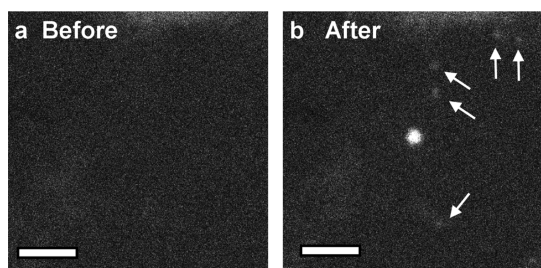
Figure 5. Area on the graphene before (a) and after (b) a growth experiment. Nuclei of dissociated precursor molecules, indicated with arrows, are scattered around the intended central deposit. The scale bars indicate 5 nm.

organometallic precursors have a low metal content, the remaining material consisting of precursor ligands that have not been removed by the electrons. For instance, Koops *et al.* used $W(CO)_6$ to create deposits with a relatively high metal content, the deposit composition being 55% W, 30% C, and 15% O.[20] Such deposits consist typically of nanocrystals (2−5 nm) embedded in a matrix of oxygen and amorphous carbon,[21] where the nanocrystals consist of W, WC, WO_2, and WO_3.[22] This is consistent with what we measured for deposits created under conditions that are similar to those we presently describe.[12] In our experiment, a less favorable degree of dissociation is considerably more likely, as the beam current is relatively low so that fewer dissociation events are expected. Also, the ADF signal during the first few steps in the growth curve is generated by molecules in the first moments after deposition when they have received a low electron dose. It is known that continued irradiation of a deposit can lead to the removal of additional ligands (such as in the case of Koops et al.).[20,23−25] This additional removal is unlikely during the initial steps in the growth curve. The minimal degree of dissociation is the loss of just one ligand, so that $W(CO)_5$ remains on the surface. For this situation, the estimated ADF voltage is 0.52 V. That gives an estimate of the most probable ADF intensity for a single dissociated $W(CO)_6$ molecule of 0.44−0.52 V.

The consistency between the expected values (0.44−0.52 V) and the experimentally obtained value (0.6 V) suggests that we observe molecule-by-molecule deposition. This demonstrates that it is possible not only to image single atoms and organometallic molecules with an electron beam[26] but also to observe the deposition of invidiual organometallic molecules. This is more than an order of magnitude beyond the state-of-the-art of other (electron) optical lithography techniques and puts FEBID in the same spatial regime as bottom-up chemistry. This can, for instance, be used for catalysis,[27] the decoration of graphene with metal for electronics,[28,29] and the controlled metal-mediated etching of graphene.[30] An important aspect of this work is that it reveals the limit of lithography with

(electron) optical systems. Figure 5 shows that nuclei are found on the graphene in the vicinity of the intentional deposit after completion of the deposition experiment. These nuclei, clusters of dissociated precursor molecules, are indicated with arrows in Figure 5b. This is caused by molecules that are adsorbed on energetically favorable positions nearby, such as defects created by the 300 keV electrons[16] or step edges. On these sites, the residence time of the precursor molecules is higher than on the pristine graphene. The longer residence time significantly increases the probability of dissociation by secondary electrons. Although the number of these nuclei outside the area illuminated by the primary electron beam is much reduced when compared to deposition on amorphous membranes, it prevents us from pushing the mass resolution limit even further and reproducibly deposit single molecules.

Finally, atom-by-atom (rather than molecule-by-molecule) deposition will be possible by exchanging $W(CO)_6$ with a fully dissociable precursor. For instance, the precursor $AuCl(PF)_3$ has been used to deposit pure gold,[31] but its thermal instability makes it very challenging to use. With the development of new and dedicated FEBID precursors, stable compounds will be found that fully decompose to pure metal and enable atom-by-atom writing with an electron beam on ultrathin supports such as (few-layer) graphene or boron nitride.

CONCLUSIONS

In conclusion, we have studied the deposition of $W(CO)_6$ on few-layer graphene with focused electron-beam-induced deposition. A dedicated scan strategy enables us to observe the deposition of the organometallic precursor *in situ* using the annular dark-field signal in a STEM. In the initial stages of the deposit growth, the recorded signal increases stepwise. The height of these steps is consistent with the expected signal for a single precursor molecule, which demonstrates that we can follow the deposition molecule-by-molecule. We observe that it takes considerably longer to deposit the first molecule on the graphene than to deposit subsequent molecules. This is explained by the fact that the residence time of the precursor molecules (prior to dissociation) is longer on the deposit than on the virgin graphene.

The scan strategy is effective when using graphene as support. On thicker (amorphous) supports, the deposits nucleate in an area that is larger than the area that can be sampled with the electron beam, so that the stepwise growth of the deposits is not observed. When graphene is used as support, isolated nuclei are observed in the vicinity of the intentional deposit after completion of a deposition experiment. Although the number of these nuclei outside the area

illuminated by the primary electron beam is much reduced when compared to deposition on amorphous membranes, it prevents us from pushing the mass resolution limit even further. Therefore, the current results present the resolution limit of (electron) optical lithography.

METHODS

Few-layer graphene is prepared by chemically exfoliating graphite, following the procedure described in refs 13−15: 10 mg of graphite in 10 mL of *N*-methyl-2-pyrrolidinone (NMP) is sonicated for 2 h at 100 W. After sonication, the suspension is centrifuged at 2000 rpm for 10 min. Droplets of the supernatant are placed on a lacey carbon membrane, supported on a Au grid (300 mesh grids, LC325-Au, Electron Microscopy Sciences). Figure S1 (Supporting Information) shows micrographs of the few-layer graphene (recorded at 80 keV) after annealing in the microscope. The flakes are distributed over the lacey carbon. The selected areas are 3−5 layers thick, determined from the number of edges that are visible.

An FEI Titan environmental STEM is used for deposition and imaging. Bright-field TEM imaging of the graphene is done at 80 keV. The settings for the acceleration voltage and spot size in STEM mode are a trade-off between beam size (imaging resolution) and probe current (signal-to-noise ratio). The microscope is operated at 300 keV and spot 7, at which 50% of the beam current is contained within 0.3 nm. The spot size is calculated for a spherical aberration of 1.2 mm, a chromatic aberration of 1.6 mm, an energy spread of 1 eV, a semiconvergence angle of 10 mrad, a geometrical probe size of 0.05 nm, and a defocus of 40 nm. The annular dark-field signal is used for all imaging, and the collecting angle is 68 mrad. The contrast/brightness settings (60.167 and 56.435%, respectively) are selected for optimal signal-to-noise ratio on the ADF signal. All pre- and postdeposition imagings are done with the standard FEI imaging software, where the ADF signal is recorded in counts.

From a National Instruments card, the scan signal is fed into the microscope *via* a switch card. The scan routine iterates between irradiating the sample with a stationary beam (duration $t_{irradiate} = 1.12 \times 10^{-1}$ s) and scanning the beam over an area of 1.8×1.8 nm, centered around the point of irradiation. The scan consists of 15×15 pixels, with a pixel size of 0.12 nm and an exposure time per pixel of 5×10^{-5} s. The total time for a single scan (t_{scan}) is 1.13×10^{-2} s, so that the condition $t_{irradiate} = 10 \times t_{scan}$ is valid. This ensures that the deposition is the result of the irradiation step, rather than the scanning step during the growth experiment. Before going to the next iteration, the electron beam is moved to a parking position while writing the recorded ADF signal to file. The ADF signal is measured at the output of the preamplifier and is recorded in volts.

The precursor is $W(CO)_6$ (CAS 14040-11-0, supplier Strem Chemicals Inc., 99% purity). The precursor is transferred to a glass vial in a nitrogen atmosphere. Before starting the deposition experiments, the reservoir is pumped for several hours and the mass spectrum is recorded. The precursor pressure during writing is 2×10^{-5} mbar. The deposition of tungsten is verified with electron energy loss spectroscopy. The scattering factor being 1.69, the intensity ratio of W to its ligands (5 CO) in the ADF signal is 5.1, which means that the ADF detection is sensitive primarily to W.

Conflict of Interest: The authors declare no competing financial interest.

Supporting Information Available: Additional figures, experimental details, and movies. This material is available free of charge *via* the Internet at http://pubs.acs.org.

REFERENCES AND NOTES

1. Keyes, R. W. The Impact of Moore's Law. *Solid State Circuits Newsletter* **2006**, *11*, 25–27.
2. Eigler, D. M.; Schweizer, E. K. Positioning Single Atoms with a Scanning Tunnelling Microscope. *Nature* **1990**, *344*, 524–526.
3. Fuechsle, M.; Miwa, J. A.; Mahapatra, S.; Ryu, H.; Lee, S.; Warschkow, O.; Hollenberg, L. C. L.; Klimeck, G.; Simmons, M. Y. A Single-Atom Transistor. *Nat. Nanotechnol.* **2012**, *7*, 242–246.
4. Duan, H.; Manfrinato, V. R.; Yang, J. K. W.; Winston, D.; Cord, B. M.; Berggren, K. K. Metrology for Electron-Beam Lithography and Resist Contrast at the Sub-10 nm Scale. *J. Vac. Sci. Technol., B* **2010**, *28*, C6H11–C6H17.
5. Van Dorp, W. F.; Hagen, C. W.; Crozier, P. A.; Kruit, P. Growth Behavior near the Ultimate Resolution of Nanometer-Scale Focused Electron Beam-Induced Deposition. *Nanotechnology* **2008**, *19*, 225305.
6. Utke, I.; Hoffman, P.; Melngailis, J. Gas-Assisted Focused Electron Beam and Ion Beam Processing and Fabrication. *J. Vac. Sci. Technol., B* **2008**, *26*, 1197–1276.
7. Botman, A.; Mulders, J. J. L.; Hagen, C. W. Creating Pure Nanostructures from Electron-Beam-Induced Deposition Using Purification Techniques: A Technology Perspective. *Nanotechnology* **2009**, *20*, 372001.
8. Van Dorp, W. F.; Hagen, C. W. A Critical Literature Review of Focused Electron Beam Induced Deposition. *J. Appl. Phys.* **2008**, *104*, 081301.
9. Van Dorp, W. F.; van Someren, B.; Hagen, C. W.; Kruit, P.; Crozier, P. A. Statistical Variation Analysis of Sub-5-nm-Sized Electron-Beam-Induced Deposits. *J. Vac. Sci. Technol., B* **2006**, *24*, 618–622.
10. Hartel, P.; Rose, H.; Dinges, C. Conditions and Reasons for Incoherent Imaging in STEM. *Ultramicroscopy* **1996**, *63*, 93–114.
11. Martin, C.; Arakawa, E. T.; Callcott, T. A.; Warmack, R. J. Attenuation Lengths of Low-Energy Electrons in Free-Standing Carbon Films. *J. Electron Spectrosc. Relat. Phenom.* **1987**, *42*, 171–175.
12. Van Dorp, W. F.; Zhang, X.; Feringa, B. L.; Wagner, J. B.; Hansen, T. W.; De Hosson, J. T. M. Nanometer-Scale Lithography on Microscopically Clean Graphene. *Nanotechnology* **2011**, *22*, 505303.
13. Hernandez, Y.; Nicolosi, V.; Lotya, M.; Blighe, F. M.; Sun, Z.; De, S.; McGovern, I. T.; Holland, B.; Byrne, M.; Gunko, Y. K.; *et al.* High Yield Production of Graphene by Liquid-Phase Exfoliation of Graphite. *Nat. Nanotechnol.* **2008**, *3*, 563–568.
14. Zhang, X. Y.; Coleman, A. C.; Katsonis, N.; Browne, W. R.; van Wees, B. J.; Feringa, B. L. Dispersion of Graphene in Ethanol Using a Simple Solvent Exchange Method. *Chem. Commun.* **2010**, *46*, 7539–7541.
15. Zhang, X. Y.; Hou, L. L.; Cnossen, A.; Coelman, A. C.; Ivashenko, O.; Rudolf, P.; Van Wees, B. J.; Brown, W. R.; Feringa, B. L. One-Pot Functionalization of Graphene with Porphyrin through Cycloaddition Reactions. *Chem.—Eur. J* **2011**, *17*, 8957–8964.
16. Egerton, R. F.; Li, P.; Malac, M. Radiation Damage in the TEM and SEM. *Micron* **2004**, *35*, 399–409.
17. Wang, Z. W.; Li, Z. Y.; Park, S. J.; Abdela, A.; Tang, D.; Palmer, R. E. Quantitative Z-Contrast Imaging in the Scanning Transmission Electron Microscope with Size-Selected Clusters. *Phys. Rev. B* **2011**, *84*, 073408.

18. Van Dorp, W. F.; Lazic, I.; Beyer, A.; Golzhauser, A.; Wagner, J. B.; Hansen, T. W.; Hagen, C. W. Ultrahigh Resolution Focused Electron Beam Induced Processing: The Effect of Substrate Thickness. *Nanotechnology* **2011**, *22*, 115303.

19. Nellist, P. D.; Pennycook, S. J. Direct Imaging of the Atomic Configuration of Ultradispersed Catalysts. *Science* **1996**, *274*, 413–415.

20. Koops, H. W. P.; Weiel, R.; Kern, D. P.; Baum, T. H. High-Resolution Electron-Beam Induced Deposition. *J. Vac. Sci. Technol., B* **1998**, *6*, 477–481.

21. Liu, Z. Q.; Mitsuishi, K.; Furuya, K. Fabrication and Investigation of Tungsten Deposit on Top and Bottom Surfaces of Thin Film Substrate. *Jpn. J. Appl. Phys.* **2007**, *46*, 6254–6257.

22. Han, M.; Mitsuishi, K.; Shimojo, M.; Furuya, K. Nanostructure Characterization of Tungsten-Containing Nanorods Deposited by Electron-Beam-Induced Chemical Vapour Decomposition. *Philos. Mag. A* **2004**, *84*, 1281–1289.

23. Botman, A.; Hagen, C. W.; Li, J.; Thiel, B. L.; Dunn, K. A.; Mulders, J. J. L.; Randolph, S.; Toth, M. Electron Postgrowth Irradiation of Platinum-Containing Nanostructures Grown by Electron-Beam-Induced Deposition from Pt(PF$_3$)$_4$. *J. Vac. Sci. Technol., B* **2009**, *27*, 2759–2763.

24. Porrati, F.; Sachser, R.; Schwalb, C. H.; Frangakis, A. S.; Huth, M. Tuning the Electrical Conductivity of Pt-Containing Granular Metals by Postgrowth Electron Irradiation. *J. Appl. Phys.* **2011**, *109*, 063715.

25. Plank, H; Kothleitner, G.; Hofer, F.; Michelitsch, S. G.; Gspan, C.; Hohenau, A.; Krenn, J. Optimization of Postgrowth Electron-Beam Curing for Focused Electron-Beam-Induced Pt Deposits. *J. Vac. Sci. Technol., B* **2011**, *29*, 051801.

26. Crewe, A. V.; Wall, J.; Langmore, T. Visibility of Single Atoms. *Science* **1970**, *168*, 1338.

27. Yoo, E. J.; Okata, T.; Akita, T.; Kohyama, M.; Nakamura, J.; Honma, I. Enhanced Electrocatalytic Activity of Pt Subnanoclusters on Graphene Nanosheet Surface. *Nano Lett.* **2009**, *9*, 2255–2259.

28. Zhao, Q. F.; Gong, J. B.; Muller, C. A. Localization Behavior of Dirac Particles in Disordered Graphene Superlattices. *Phys. Rev. B* **2012**, *85*, 104201.

29. Rodriguez-Manzo, J. A.; Cretu, O.; Banhart, F. Trapping of Metal Atoms in Vacancies of Carbon Nanotubes and Graphene. *ACS Nano* **2010**, *4*, 3422.

30. Ramasse, Q. M.; Zan, R.; Bangert, U.; Boukhvalov, D. W.; Son, Y. W.; Novoselov, K. S. Direct Experimental Evidence of Metal-Mediated Etching of Suspended Graphene. *ACS Nano* **2012**, *6*, 4063.

31. Utke, I.; Hoffmann, P.; Dwir, B.; Leifer, K.; Kapon, E.; Doppelt, P. Focused Electron Beam Induced Deposition of Gold. *J. Vac. Sci. Technol., B* **2000**, *18*, 3168.